
Article:
González-Nicolás, A., Bau, D. orcid.org/0000-0002-0730-5478 and Cody, B.M. (2017) Application of Binary Permeability Fields for the Study of CO 2 Leakage from Geological Carbon Storage in Saline Aquifers of the Michigan Basin. Mathematical Geosciences. ISSN 1874-8961

https://doi.org/10.1007/s11004-017-9706-x

Application of Binary Permeability Fields for the Study of CO_2 Leakage from Geological Carbon Storage in Saline Aquifers of the Michigan Basin[1]

Ana González-Nicolás[1,2,*], Domenico Baù[3], Brent M. Cody[4]

[1] Energy Geosciences Division, Lawrence Berkeley National Laboratory, University of California, Berkeley, CA, USA

[2] Now at Institute for Modelling Hydraulic and Environmental Systems (LS[3])/SimTech, University of Stuttgart, Stuttgart, Germany

[3] University of Sheffield, Department of Civil and Structural Engineering, Sheffield, UK,

[4] Natural Resources Consulting Engineers Inc., Fort Collins, CO, USA

*Corresponding author: T: +49 711 685-60109

Mail address: Institute for Modelling Hydraulic and Environmental Systems (LS3)/SimTech Pfaffenwaldring 5a, D-70569 Stuttgart

E-mail address: anagna@gmail.com (A. González-Nicolás)

orcid iD 0000-0003-2869-8255

Abstract

The feasibility of geological carbon storage sites depends on their capacity to safely retain CO_2. While deep saline formations and depleted gas/oil reservoirs are good candidates to sequester CO_2, gas/oil reservoirs typically have a limited storage capacity (~1 Mt/year) compared to alternative targets considered for CO_2 disposal (Celia et al. 2015). In this respect, deep saline aquifers are considered more appropriate formations for geological carbon storage but present the disadvantage of having limited characterization data. In particular, information about the

[1] Accepted for publication in Mathematical Geoscience (DOI 10.1007/s11004-017-9706-x). Available online here.

continuity of the overlying sealing formations (caprock) is often sparse if it exists at all. In this work, a study of CO_2 leakage is conducted for a candidate geological carbon storage (GCS) site located in the Michigan Basin, whose sealing properties of the caprock are practically unknown. Quantification of uncertainty on CO_2 leakage from the storage formation is achieved through a Monte Carlo simulation approach, relying on the use of a computationally efficient semi-analytical leakage model based upon the solution derived by Nordbotten et al. (2009), which assumes leakage occurs across "passive" wells intersecting caprock layers. A categorical indicator Kriging simulator is developed and implemented to represent the caprock sealing properties and model the permeability uncertainty. Binary fields of caprock permeability are generated and exhibit mostly low permeability, with sparsely-occurring local high permeability areas where brine and CO_2 may leak out of the storage formation. In addition, the feasibility of extending the use of the semi-analytical model to large-area leakage pathways is studied. This work advances a methodology for preliminary uncertainty quantification of CO_2 leakage at sites of GCS with little or no information on the sealing properties of the caprock. The implemented analysis shows that, for the considered site, CO_2 leakage may not be negligible even for relatively low (~1%) probabilities of finding permeable inclusions in the caprock and highlights the importance of being able to characterize caprock sealing properties over large areas.

Keywords: Categorical indicator Kriging simulator; CO_2 leakage; CO_2 storage; Semi-analytical solution.

1 Introduction

Increases in average global air and ocean temperatures are documented around the world with a global mean annual surface temperature increase of 0.3-0.6ºC since the late 19th century (Nicholls et al. 1996). This phenomenon is due to the proliferation of greenhouse gas concentrations from anthropogenic emissions, particularly from carbon dioxide (CO_2), the most important greenhouse gas produced by human activities (IPCC 2007). To stabilize CO_2 emissions into the atmosphere several strategies have been suggested, among them geological carbon storage (GCS). GCS is advanced as a promising approach to reduce CO_2 emissions from power

53 plants without needing to switch fuel sources (IPCC 2005). Suitable reservoirs for GCS are deep
54 saline formations, depleted oil and gas reservoirs, and unmineable coal seams (Bergman and
55 Winter 1995; Bachu 2003; Ruether 1998). Deep saline formations are widespread and offer 60%
56 of the estimated storage capacity (IEA 2008). However, compared to oil and gas reservoirs, they
57 lack characterization data and available information about their geological properties is usually
58 scarce.

59 One of the requirements for GCS is the presence of a sealing formation that prevents
60 stored CO_2 from escaping from the injected formation (IPCC 2005) and guarantees a long term
61 sequestration. Deep saline aquifers have the inconvenience of being typically unexplored.
62 Accordingly, little is known about the properties of the sealing formations, which are potentially
63 compromised by the presence of leakage pathways, such as faults or fractures, permeable areas
64 of the caprock, and poorly completed existing wells (IPCC 2005).

65 Several studies that investigate the importance of CO_2 leakage associated with faults and
66 existing wells have been documented. For instance, Chang et al. (2008) studied the CO_2 leakage
67 through faults where flow properties of faults are uncertain. They found that lateral CO_2 migration
68 through overlying permeable formations attenuates CO_2 leakage through faults. The effect of
69 faults, fault permeability, and flow velocity of groundwater on the migration of a CO_2 plume was
70 studied by Sakamoto et al. (2011). Zhang et al. (2010) proposed a method to calculate the
71 probability of CO_2 leakage through fractures and faults in a two-dimensional system. In high well-
72 density areas, abandoned wells may represent a significant escape pathway for the injected CO_2.
73 Gasda et al. (2004) observed that a CO_2 plume could impact twenty to several hundred abandoned
74 wells depending on the well density. Kopp et al. (2010) concluded that high risk of leakage
75 through abandoned wells was produced by long injection times, small distances between injection
76 wells and leaky wells, high permeability anisotropy, high geothermal gradient, and low depth. In
77 Celia et al. (2011), the permeability of abandoned wells was identified as the most influential
78 parameter resulting in CO_2 leakage from GCS. Nogues et al. (2012) implemented a Monte Carlo
79 simulation where the main uncertainty was the effective well permeability. They showed that
80 results on leakage depended on formation properties, location, and number of leaky wells.

In González-Nicolás et al. (2015a), stochastic and global sensitivity analyses were applied to study different types of uncertainty affecting leakage of CO_2 through passive wells during GCS operations for a potential candidate site located in the Michigan Basin. In this work, the investigation of González-Nicolás et al. (2015a) is extended to include the presence of potential areas of high permeability of the caprock potentially much larger than passive wells. The level of uncertainty is significantly increased since the location of passive wells is known, whereas the location, the size and the spatial frequency of caprock discontinuities are practically unknown. A probabilistic study of CO_2 leakage is performed by applying a Monte Carlo simulation approach, where the main source of uncertainty is the caprock permeability. "Weak" areas of the sealing formation are herein considered as localized depositions of higher permeability materials and referred to as "inclusions".

A categorical indicator Kriging simulation algorithm is applied to generate ensembles of realizations of the caprock permeability field with two types of facies: 1) sealing formation (areas with low permeability), and 2) inclusions (areas with high permeability). The caprock permeability ensemble is thus used in a Monte Carlo analysis to perform a stochastic simulation of CO_2 injection and probabilistically quantify leakage through the weak caprock areas. Due to the unavailability of geological data with sufficient resolution, different geostatistical configurations for the sealing formation are studied to assess the impact of the uncertainty of caprock inclusions on the probability of CO_2 leakage. Areas of high permeability having relatively similar spatial locations are grouped together into clusters to reduce the number of leaky points used by the semi-analytical multiphase flow model, thus reducing the computational effort. To understand the potential limitations of the clustering approach, results from the semi-analytical multiphase flow model are compared with those obtained using a numerical model. Also, the influence of CO_2 leakage through existing abandoned wells located in the area of interest is studied.

The organization of this paper is as follows. First, the methodology of the study is described, which includes the multiphase flow semi-analytical algorithm, the generation of binary

permeability fields, and the statistical analysis. Then the application of the methodology to the Michigan Basin test site and results are presented. Lastly, a summary of conclusions is given.

2 Methodology

2.1 Multiphase Flow Semi-Analytical Model

ELSA-IGPS (Baù et al. 2015) is a multiphase flow simulator based upon the semi-analytical model ELSA developed by Celia and Nordbotten (2009) and Nordbotten et al. (2009). ELSA-IGPS is able to simulate the injection of supercritical CO_2 into a deep saline formation and compute the leakage of brine and CO_2 through poorly-sealed, "passive" wells. The domain is structured as a stack of horizontal, homogeneous, and isotropic aquifers separated by caprock layers, and perforated by a generic number of CO_2 injection wells and passive wells. CO_2 injection rates are assumed to be constant during the injection period, and no post-injection phase is simulated. Caprock layers are impermeable except at passive well locations. Initially, the domain is saturated with brine at hydrostatic pressure. Flow is assumed to be horizontal in aquifers and vertical in passive wells. Capillary pressure, dissolution and chemical reactions are neglected. The model considers a brine relative permeability equal to one in areas where no CO_2 is present, whereas in areas invaded by the CO_2 plume, the relative permeability of CO_2 is given by the end-point CO_2 relative permeability, which depends on the residual saturation of brine. The effective compressibility is assumed to be equal to the brine compressibility since most of the domain is filled with brine (Nordbotten et al. 2009). More details about the model assumptions can be found in Celia and Nordbotten (2009).

In ELSA (Nordbotten et al. 2005), fluid pressures changes are the compound effect of CO_2 injection and fluid leakage across caprock layers in passive wells. To determine the fluid overpressure, superposition of effects is applied based on a fundamental "well" function given in Celia et al. (2011). Using this approach, the fluid pressures $p_{j,l}$ at the bottom of each aquifer l (l=1,2,..,L; L denotes the number of aquifers), at each passive well j (j=1,2,..,N; N denotes the number of passive wells), and at any given time t are non-linear functions of the fluid densities,

viscosities, and compressibility, as well as the thickness, porosity, brine residual saturation and permeability of the aquifers. These functions also depend on CO_2 injection rates entering aquifer l from each of the passive wells j. The cumulative fluid masses $M_{j,l}(t)$ are calculated as

$$M_{j,l}(t) = \int_0^t \rho_{eff,j,l}(\tau)\left[Q_{j,l}(\tau) - Q_{j,l+1}(\tau)\right]d\tau, \quad (1)$$

where Q is the volumetric flow rate [L^3T^{-1}] and ρ_{eff} is the effective fluid density [ML^{-3}]. This density is time-dependent since the composition of the leaking fluid varies upon the CO_2 plume location. To calculate leakage rates $Q_{j,l}$, Nordbotten et al. (2005) propose to use the sum of the flow rates $Q_{\alpha\,j,l}$ for each phase α (b for brine and c for CO_2) given by a multiphase version of Darcy's law

$$Q_{j,l} = \sum_{\alpha=b,c}\left[\pi r_{pw\,j,l}^2 \frac{k_{r,\alpha\,j,l}k_{pw\,j,l}}{\mu_\alpha B_l}\left(p_{j,l-1} - \rho_\alpha g B_l - p_{j,l} - \rho_\alpha g H_{l-1}\right)\right]. \quad (2)$$

In Eq. (2), r_{pw} is the passive well radius [L], k_{pw} is the single-phase passive well permeability [L^2], μ_α is the dynamic viscosity of α [$ML^{-1}T^{-1}$], B is the aquitard thickness [L], p is the pressure at the bottom of an aquifer [$ML^{-1}T^{-2}$], g is the gravitational acceleration [LT^{-2}] and H is the aquifer thickness [L].

The substitution of Eqs. (1) and (2) in the expression of fluid pressures $p_{j,l}$ leads to a system of non-linear equations. In ELSA-IGPS (Baù et al. 2015), this system is efficiently solved using a fixed-point scheme, which leads to a substantial computational saving when compared to the linearization scheme adopted in ELSA by Nordbotten et al. (2005). Further details about the model equations and solving procedures are given in Baù et al. (2015) and González-Nicolás et al. (2015a).

2.2 Binary Permeability Fields

2.2.1 Generation of Binary Permeability Fields

Equally likely realizations of the caprock permeability spatial distribution are generated with a categorical indicator Kriging simulator (CIKSIM), relying on a sequential Gaussian simulation algorithm similar to that implemented in the "sgsim" routine available in the Geostatistical Software Library (GSLIB) software developed by Deutsch and Journel (1998).

158 CIKSIM (González-Nicolás et al. 2015b) is based on a "multi-point" categorical geostatistics and
159 has been developed to generate generic facies distributions characterized by arbitrary (continuous
160 or discontinuous) and stationary local probability distribution functions (PDFs) and covariograms
161 that may differ from category to category. CIKSIM approximates a generic cumulative
162 probability distribution function (CDF) using a piecewise linear function. At any point in space
163 during the simulation, the estimated conditional probabilities of the categories are used to
164 randomly select the property values using the inverse CDF.

165 Note that other algorithms are available to generate caprock permeability field based on
166 generic, non-Gaussian, CDFs such as those based on the normal score transform (Goovaerts 1997;
167 Deutsch and Journel 1998) and Gaussian mixtures (Grana et al. 2012). For the purposes of this
168 study, CIKSIM is used to create binary fields that include two types of facies (or categories).
169 Facies 1 represents caprock areas with little or no permeability, and facies 2 represents inclusions
170 characterized by a high permeability. Thus, CIKSIM generates inclusions of the caprock to
171 introduce in the multiphase flow semi-analytical model explained in Sect. 2.1. The caprock
172 permeability k is represented as a binary field (Deutsch and Journel 1998)

$$k(\boldsymbol{u}) = k_1 I(\boldsymbol{u}) + k_2[1 - I(\boldsymbol{u})], \tag{3}$$

173 where k_1 and k_2 are the permeabilities of facies 1 and facies 2, respectively, at position $\boldsymbol{u}$, and I
174 is the indicator transform.

175 *2.2.2 Clustering of Inclusions*

176 If a large number of inclusions is generated for each field of the ensemble, the
177 computational cost required by running the semi-analytical flow model (Sect. 2.1) will increase.
178 To reduce this cost, a clustering algorithm of the inclusions is developed. A cluster is considered
179 when two or more inclusion gridblocks are "in contact", that is, when the distance between the
180 centers of their gridblocks is less or equal to $\sqrt{2} \cdot \Delta x$, where Δx is the gridblock size adopted in
181 the generation of the k field. The size and distribution of these clusters depend on the parameters
182 assigned for their generation. In the semi-analytical model, each cluster is modeled as a single
183 circular leakage spot (passive well) with an area equivalent to that of the cluster itself. The

184 position of the leakage spot is calculated as the centroid of the gridblocks forming the cluster.
185 One example of grouping the clusters at the caprock is shown in Fig. 1. In this example, the
186 number of 84 inclusions-blocks (orange gridblocks) is reduced to only 16 clusters after applying
187 the clustering approach. The equivalent areas of the clusters are shown as black circles in Fig. 1.
188 Each of these clusters is used as a single leaky point in the semi-analytical model ELSA-IGPS of
189 Sect. 2.1.
190 [Figure 1 here]
191 Originally, ELSA-IGPS was developed to simulate multi-phase flow and estimate the
192 leakage of both brine and CO_2 flux along existing passive wells. That is to say, leakage always
193 occurs through small cross-sectional areas of the caprock (radii between 0.15 m – 1 m). In
194 contrast, here, ELSA-IGPS is used to simulate escapes through larger weak areas of the caprock.
195 A comparison with a numerical code is made to understand the limitations of using the semi-
196 analytical model in this way. The comparison is carried out using the compositional version E300
197 of ECLIPSE (Schlumberger 2010). ECLIPSE is a commercial numerical multi-phase flow model
198 based on a three-dimensional finite-difference discretization and widely used in the gas and oil
199 industry.
200 It is worth noting that the clustering approach is likely to alter the geostatistics of the
201 inclusions and, in particular, their variogram. However, the most important requirement for this
202 study is to maintain accuracy in the estimation of CO_2 leakage, as explained above, rather than
203 preserving the geostatistics of the caprock.

204 2.3 Statistical Analysis

205 In this work, CO_2 leakage through caprock discontinuities and passive wells is quantified
206 as the percentage of CO_2 mass, $\%M_{leak}$, released into aquifers overlying the targeted storage
207 formation with respect to the total mass of CO_2 injected. CO_2 injection takes place in the deepest
208 formation (l=1) through a single injection well (M=1), with only one overlying aquifer (l=2)
209 above the injected aquifer considered (more details on the conceptual model are in Sect. 3.1).

210 $\%M_{leak}$ is calculated as the ratio between the mass of CO_2 that escapes from the injected
211 formation into layer l=2 and the total CO_2 injected into layer l=1 at final time t_{end}

$$\%M_{leak} = \frac{M_{leak}(t_{end})}{\rho_c Q_{1,1} t_{end}} 100, \quad (4)$$

212 where $M_{leak}(t_{end})$ is given by the net cumulative CO_2 mass transferred into aquifer l=2 through
213 all passive wells j (j=1,2,…,N)

$$M_{leak}(t_{end}) = \int_0^{t_{end}} \left[\sum_{j=1}^{N} \rho_c s_{c,j,2}(\tau) Q_{j,2}(\tau)\right] d\tau. \quad (5)$$

214 In Eq. (5) $s_{c,j,2}$ represents saturation of CO_2 at passive well j and aquifer l=2.

215 Output ensembles of the state variable $\%M_{leak}$ are used to produce CDF plots. A CDF
216 of the state variable $\%M_{leak}$ is obtained from the output of N_{MC} model simulations. After ordering
217 the $\%M_{leak}$ values in ascending order, $\%M_{leak_1} < \%M_{leak_2} < \cdots < \%M_{leak_{N_{MC}}}$, the
218 corresponding CDF values are calculated as $CDF(\%M_{leak}) = (i - 0.5)/N_{MC}$ (i=1,2,…,N_{MC})
219 (Hahn 1967). To optimize the performance of the simulations, preliminary tests are run to find
220 the minimum ensemble size N_{MC} beyond which CDFs remain substantially stationary. A sample
221 size of N_{MC}= 500 is selected for each of the investigated scenarios.

222 The methodology applied in this study is summarized as follows. First, CIKSIM is
223 applied to the grid domain using conditional facies data, such as possible information on caprock
224 sealing properties in given areas. As a result, an ensemble of caprock binary fields containing the
225 two types of facies is obtained. The clustering approach is then applied to the caprock binary
226 fields in order to decrease the number of leaky areas to be introduced in the multiphase flow semi-
227 analytical model. After the completion of the clustering process, ELSA-IGPS Monte Carlo
228 simulations are run and a statistical analysis of the output ensembles of mass leakage are used to
229 generate CDF profiles. Figure 2 shows a flowchart of such methodology.

230 [Figure 2 here]

3 Application to the Michigan Basin Test Site

3.1 Study Area

The methodology introduced in Sect. 2 is applied to a geological test site located within the Michigan Basin in proximity to the town of Thompsonville, MI. The candidate formation proposed for GCS is known as the Gray Niagaran formation. Fig. 3 shows a cross-section of the Michigan basin in the area of interest with the candidate storage formation highlighted in yellow. The Gray Niagaran formation lies below an almost depleted hydrocarbon reservoir (Brown Niagaran pinnacle in Fig. 3), which is currently used by Michigan Technological University for geophysical research.

[Figure 3 here]

The Gray Niagaran formation has a thickness of 119 m with its top at 1,500 m below the ground surface, making this formation appropriate as a geological repository of CO_2. The choice to store supercritical CO_2 in this formation is justified by the sealing capacity of the formations above the Brown Niagaran pinnacle. However, a relevant source of uncertainty lies in the continuity of the caprock, highlighted in Fig. 3 (green shading). Although several data are available from monitoring wells at the test site (Halliburton 1990; SCH 1983, 1991), the information that can be used directly to describe the spatial distribution of the sealing properties of the caprock formation at the basin scale is scarce.

The model system is conceptualized in ELSA-IGPS as a stack of two aquifers (L=2): the Gray Niagaran formation (119 m thick) below and the Carbonate formation (35 m thick) above. The two aquifers are separated by a 17-m thick caprock layer constituted by marine evaporites (Fig. 3). Supercritical CO_2 is injected into the Gray Niagaran formation through a single well.

When using the numerical simulator ECLIPSE, the geological model is also conceptualized as two aquifers separated by a caprock, with the same thicknesses described above. The model domain is divided into 100 m × 100 m gridblocks horizontally. Vertically, each formation is divided into four sub-layers. A single vertical CO_2 injection well is modeled at the center of the domain and screened within the lower aquifer. The grid resolution in the area

surrounding the injection well is progressively increased to achieve an appropriate size for a well (about 0.5 m). To simulate a laterally infinite aquifer system, the pore volume of the boundary gridblocks is multiplied by a factor of 1×10^6. In order to obtain comparable results with ELSA-IGPS, the CO2SOL option of ECLIPSE is selected, which models the flow of two immiscible fluids with no capillary pressure.

In both models, ELSA-IGPS and ECLIPSE, the mass injection rate is Q_m= 30 kg/s (about 0.95 Mt/year) and remains constant during a simulated period of 10 years (t_{end} in Eq. (5)). Initially, all formations are assumed to be saturated only with brine and under hydrostatic pressure conditions. The caprock is assumed impermeable except for the location of inclusions or passive wells located in the area of interest. A Van Genuchten constitutive model (Van Genuchten 1980) is used to calculate relative permeabilities of CO_2 and brine, assuming a brine residual saturation s_b^{res}=0.3 and a fitting parameter of 0.41 (Zhou et al. 2009). Porosity values are extracted from the log-wells of the two boreholes in Fig. 3 (Halliburton 1990; SCH 1983, 1991). The injected aquifer and the overlying formation are assumed to have a permeability equal to 2.8×10^{-14} m^2 and 9.6×10^{-15} m^2, respectively, calculated according to Trebin (1945) as

$$\begin{aligned} k &= 2e^{31.6\varphi} && \text{if } 100\varphi < 12\% \\ k &= 4.94(100\varphi)^2 - 763 && \text{if } 100\varphi > 12\% \end{aligned} \quad , \tag{6}$$

where: k is the permeability in millidarcy (mD, 1mD ≡ 1×10^{-15} m^2), and φ is the porosity (/). For the comparison of ELSA-GPS and ECLIPSE results, the sealing formation is assigned a permeability k_1=0. For simplicity, inclusions in the caprock are assumed to have the same permeability as the injected aquifer l=1 ($k_2 = k_{l_1}$). The hydro-geomechanical parameters used in this study are provided in Table 1.

[Table 1 here]

3.2 Caprock Permeability Generation

In order to generate caprock permeability realizations, CIKSIM is used. For this purpose, a grid covering an area of 7 km × 7 km is considered with the hydrocarbon reservoir located at its center (Fig. 1). Each gridblock is 100 m × 100 m, yielding a total of 4,900 blocks. The thickness

283 of the caprock above the Gray Niagaran formation is relatively small when compared to the
284 horizontal extension of this formation (30.5 m thickness of caprock versus 7,000 m of estimated
285 grid extension), thus the permeability is represented as a two-dimensional heterogeneous field
286 with no variation in the vertical direction.

287 Since the reservoir has contained oil before, it is assumed that the caprock in its area is
288 perfectly impermeable. This information is used to "condition" caprock permeability realizations
289 as facies 1 in the gridblocks inside the reservoir boundary. The caprock permeability in the other
290 gridblocks (unsampled locations) is unknown and thus simulated stochastically. In Fig. 1, the
291 lateral boundary of the reservoir is indicated by the blue line, and red dots correspond to
292 gridblocks where the permeability is that of facies 1.

293 *3.2.1 Uncertainty from Caprock Continuity*

294 The generation of the caprock permeability ensembles with CIKSIM is based on the two-
295 point geostatistics described in Table 2. The following exponential covariance model is used for
296 both facies

$$C_{k_i k_i}(d; \sigma_{k_i}^2, l_{k_i}) = \sigma_{k_i}^2 exp\left(-\frac{d}{l_{k_i}}\right) \quad (i = 1,2), \tag{7}$$

297 where: d is the horizontal distance between any two points; $\sigma_{k_1}^2$, $\sigma_{k_2}^2$, and l_{k_1}, l_{k_2} are the variances
298 and the correlation lengths of the two facies; and k_1 and k_2 are the permeability of facies 1 and
299 2, respectively. Note that $\sigma_{k_1}^2 = P_1(1 - P_1)$ and $\sigma_{k_2}^2 = P_2(1 - P_2)$, where P_1 and P_2 are the
300 probability of facies 1 and 2, respectively. Several probabilities of the occurrence of P_2 are applied
301 for facies 2 (inclusions) ranging between 0.0005 and 0.02, as well as correlation lengths $l_{k_2} = l_{xy}$
302 ranging between 200 m and 1,500 m (xy denotes equal correlation lengths in the x and y
303 directions. Facies 1 has a probability $P_1 = 1 - P_2$, and a correlation length l_{k_1}= 1,000 m in all
304 scenarios. N_{MC} in Table 2 refers to the ensemble size.

305 [Table 2 here]

306 To analyze the caprock permeability field generated by CIKSIM in relation to the
307 correlation length l_{xy} and the effect that this has on CO_2 leakage, two parameters are here

308 introduced: the average distance D between the inclusion clusters and the injection well; and the
309 inclusion ratio r_{lc}. The distance D is calculated as

$$D = \frac{1}{N_{MC}} \sum_{j=1}^{N_{MC}} \frac{\sum_{i=1}^{N_{cl}} d_{i,j}}{N_{cl}}, \quad (8)$$

310 where N_{cl} (i=1,2,.., N_{cl}) is the total number of clusters present in realization j (j=1,2,.., N_{MC}), and
311 $d_{i,j}$ is the distance between the center of the cluster i in realization j and the injection well. In
312 general, one can expect CO_2 leakage to be probabilistically more pronounced for smaller values
313 of D, which practically indicates how close to the injection well the inclusions are on average.
314 The inclusion ratio r_{lc} is defined as the fraction between the average number of actual
315 inclusion blocks generated in the ensemble and the expected number of inclusion blocks

$$r_{lc} = \frac{\frac{\sum_{j=1}^{N_{MC}} l_{c,j}}{N_{MC}}}{P_2 N_{gb}}, \quad (9)$$

316 where N_{gb} is the total number of gridblocks considered for the generation of the caprock (N_{gb}=
317 4,900), and $l_{c,j}$ is the number of inclusion gridblocks in realization j. For instance, for a
318 probability P_2= 0.01, the expected number of inclusion blocks is 49 ($P_2 N_{gb}$). In general, larger
319 r_{lc} values indicate the presence of larger inclusions than expected, which should probabilistically
320 produce larger CO_2 leakage.
321 Finally, to investigate the influence of the injected formation permeability and inclusions
322 permeability on CO_2 leakage, different combinations of these are considered as in the scenarios
323 1.1, 2.1, 3.1, 4.1, and 5.1 presented in Table 2. The range of permeabilities of the injected
324 formation k_{l_1} and inclusions k_2 studied spans from 1×10^{-15} m^2 (about 1 mD) to 1×10^{-12} m^2 (about
325 1,000 mD). Results of these analyses are reported in terms of the 95th percentile of $\%M_{leak}$ (Eq.
326 (4)).

327 *3.2.2 Uncertainty from Caprock Continuity and Passive Wells Permeability*

328 The study area considered in Sect. 3.1 comprises 60 wells that perforate the candidate
329 formation to store CO_2. The locations of these wells are obtained from the Michigan Department
330 of Environmental Quality database (MDEQOGD 2014). The integrity of these wells is uncertain.

A deteriorated or poorly cemented well can create a leaky pathway for brine and/or CO_2. Since the number of these passive wells is significant, they are included in the uncertainty analysis for CO_2 leakage.

Before use in the semi-analytical model, these 60 passive wells are grouped into 20 equivalent leaky pathways following the approach outlined in González-Nicolás et al. (2015a). Following this approach, these groups are identified by minimizing the sum of the Euclidean distances of the passive wells that form a cluster of wells and the cluster centroid. The equivalent leaky area considered for each cluster of wells is equal to the sum of the cross-sectional areas of the wells included in that group. From the equivalent leaky area, an equivalent radius is calculated and introduced into Eq. (2) to compute the flow rate through this cluster. Figure 4 shows the positions of the 60 passive wells and the position of the 20 equivalent groups of wells after clustering.

[Figure 4 here]

The location of these well groups is fixed in each of the realizations of the caprock permeability, but their permeability is considered stochastic, as no information is available on passive well integrity. All passive well permeabilities are assumed to fit to the same lognormal probability distribution function with a log-mean of $\log(1\times10^{-14}\ m^2)$ and a log-standard deviation of 1 log-m^2 (Nordbotten et al. 2009).

4 Results and Discussion

4.1 Simulating CO_2 Leakage from Large Caprock Areas Using ELSA-IGPS

To investigate the viability of simulating CO_2 leakage across generic caprock inclusions with the semi-analytical model, results of ELSA-IGPS are compared with those of the numerical model ECLIPSE. Results of the comparison are summarized in Fig. 5 and Fig. 6.

Figure 5 presents the cumulative mass leakage of CO_2 over time for two representative caprock permeability realizations from scenario 3.1. These two realizations are shown in Fig. 5a and 5b, whereas the corresponding CO_2 leakage profiles are shown in Fig. 5c and 5d. In both

357 realizations, the final (at t_{end} =10 years) cumulative CO_2 mass leakage given by ELSA-IGPS
358 and that given by ECLIPSE are quite similar. In addition, the final cumulative CO_2 mass leakages
359 in the two realizations are of the same order of magnitude. However, for the realization in Fig.
360 5a, the CO_2 mass leakage simulated by ECLIPSE starts earlier than that obtained with ELSA-
361 IGPS (Fig. 5c). These differences are not observed in Fig. 5d, which relates to the realization
362 shown in Fig. 5b.

363 [Figure 5 here]

364 The analysis of the two models' results for several other realizations of the caprock
365 permeability (results not shown here) suggests that ECLIPSE simulates consistently an earlier
366 CO_2 leakage than ELSA-IGPS's when caprock discontinuities are located farther away from the
367 CO_2 injection well. In this respect, a major difference between the realizations in Figs. 5a and 5b
368 lies in the distance at which the closest inclusion to the CO_2 injection well is found. In Fig. 5a
369 such distance is 1,532 m, whereas in Fig. 5b it is 526 m. Numerical tests conducted in this study
370 show that this distance is a crucial parameter for the comparison, and discrepancies between the
371 two models, in terms of CO_2 leakage versus time, are observed only when this minimum distance
372 is greater than about 600 m (Figs. 4a and 4c). For realizations having the closest inclusion within
373 600 m (Fig. 5b) no substantial difference in the CO_2 mass leakage profiles is found (Fig. 5d).
374 The earlier CO_2 leakage simulated by ECLIPSE as compared to ELSA-IGPS has already
375 been observed by Nordbotten et al. (2009), who attributed these differences to numerical diffusion
376 in ECLIPSE. Our results confirm these observations. Effects of numerical diffusion lead to
377 simulating a more spread out CO_2 plume front at any given time, that is, a CO_2 plume that
378 somehow advances faster. This results in an earlier leakage, particularly when inclusions are
379 located farther away from the injection well, since in this case the CO_2 plume has to travel longer
380 distances before leakage starts, exacerbating the effects of numerical diffusion.

381 Figure 6 shows the CDF of $\%M_{leak}$ (Eq. (4)) of ELSA-IGPS (in red) and ECLIPSE (in
382 blue) for scenarios 2.1 (dashed lines) and scenario 4.1 (solid lines). One can observe that CO_2
383 mass leakage for the two codes is quite similar for $\%M_{leak}$ values greater than 1%, whereas larger

discrepancies are found for smaller $\%M_{leak}$ values. Also, differences in CO_2 leakage are more pronounced for larger inclusion probabilities P_2. Statistically, ECLIPSE produces more leakage of CO_2 than ELSA-IGPS, which can also be explained by the effects of numerical diffusion discussed above. The analysis of the CDFs in Fig. 6 reveals that low ranges of $\%M_{leak}$ are characterized by realizations with inclusions located farther away from the injection well, in which the CO_2 leakage simulated by ELSA-IGPS starts later than ECLIPSE's, thus producing a lower $\%M_{leak}$.

[Figure 6 here]

In general, the cumulative CO_2 mass leakage produced by the two models is of the same order of magnitude at later times, hence showing a reasonably good agreement between the two approaches. But since the computational cost of ELSA-IGPS is about two/three orders of magnitude lower than ECLIPSE's, the advantage achieved by introducing clustered inclusions into ELSA-IGPS is quite significant for quantifying the uncertainty on CO_2 leakage at the considered site.

4.2 Quantifying Uncertainty on Caprock Continuity

4.2.1 Testing of Binary Permeability Fields

Figure 7 shows profiles of the average distance D (Eq. (8)) and the inclusion ratio r_{lc} (Eq. (9)) as functions of the correlation length l_{xy}. In Fig. 7a, the D versus l_{xy} relationship is graphed for probabilities P_2 equal to 0.005, 0.01, and 0.02. In general, as the correlation length l_{xy} of facies 2 increases, the distance D is observed to decrease at first and then become roughly constant. In practice, low correlation lengths lead to generating smaller inclusions, generally spread out throughout the domain and thus situated – on average – farther away from the injection well. On the other hand, larger correlation lengths signify larger inclusions, which are constrained within the domain and thus lead to smaller values of D. As a result, for a given probability P_2 and different correlation lengths, larger l_{xy} values will reflect larger CO_2 mass leakage because the

409 average distance D that the CO_2 plume has to travel through the storage formation to reach
410 caprock inclusions, and thus the travel time, will be shorter.

411 [Figure 7 here]

412 Figure 7b displays the relationship between correlation length l_{xy} and the inclusion ratio
413 r_{lc} for probabilities P_2 equal to 0.005, 0.01, and 0.02. This figure shows that in general r_{lc} is equal
414 to 1 only when the correlation length is very small (l_{xy}= 0.1 m) and exhibits a general increasing
415 trend as l_{xy} increases. This trend is, however, not significant for correlation lengths l_{xy} beyond
416 400 m, where r_{lc} becomes roughly constant with values oscillating between 1.6 and 1.8 depending
417 on the assigned probability P_2. This indicates that, in order to simulate caprock continuity and its
418 impact on the uncertainty on CO_2 leakage, assigning meaningful values of the correlation l_{xy} can
419 be as significant as assessing the inclusion probability P_2.

420 *4.2.2 Quantifying CO_2 Leakage*

421 The effects of the correlation length l_{xy} and the inclusion probability of facies 2 on CO_2
422 leakage are summarized in Fig. 8, which shows the CDF of $\%M_{leak}$ (Eq. (4)) for some of the
423 scenarios described in Table 2. In general, CO_2 mass leakage is higher for larger P_2 values. This
424 is not surprising, since a higher P_2 substantially means a higher probability of the CO_2 plume to
425 encounter leakage pathways across the caprock. It is interesting to observe, however, that if a
426 maximum $\%M_{leak}$ target of 1×10^{-3} is prescribed, this is met with an 81% probability in scenario
427 1.1 (P_2= 0.0005 and l_{xy}= 200 m) and only with a 1% probability in scenario 5.1 (P_2= 0.02 and
428 l_{xy}= 200 m).

429 [Figure 8 here]

430 Results in Fig. 7 confirm that the $\%M_{leak}$ associated to caprock permeability fields with
431 the same probability P_2 is larger for larger correlation lengths, since inclusions have larger extent
432 and, consequently, the CO_2 mass leakage is more likely to occur. This is in agreement with two
433 points made previously: i) the distance from the center cluster to the injection well D is lower for

434 a higher correlation length (Fig. 7a); and ii) the inclusion ratio is greater for higher correlation
435 lengths (Fig. 7b). For example, there are, on average, more inclusions in a scenario where l_{xy}=
436 1,500 m, than when l_{xy}= 200 m, and the distance that the CO_2 plume has to travel to reach the
437 center of inclusion clusters is shorter, thus promoting earlier leakage of CO_2.

438 *4.2.3 Influence of Permeability Values of the Injected Formation and Inclusions*

439 To study the combined influence of the storage formation permeability k_{l_1} and the
440 inclusions permeability k_2 on the maximum probable amount of leaked CO_2, different
441 combinations of k_{l_1} and k_2 are considered for scenarios 1.1, 2.1, 3.1, 4.1, and 5.1 (Table 2). These
442 results are presented in Fig. 9, which shows contour maps of the $\%M_{leak}$ 95th percentile as a
443 function of k_{l_1} and k_2. Each subpanel in Fig. 9 corresponds to one of the scenarios above. All
444 scenarios exhibit the lowest CO_2 mass leakage when k_{l_1} is high and k_2 is low. In general, high
445 permeability of the injection formation $corresponds$ to less escape of CO_2 through weak areas.
446 The CO_2 plume advances more easily through the injected formation when k_{l_1} is high, which
447 enhances its injectivity and storage properties, and limits CO_2 escape, particularly if the inclusion
448 permeability k_2 is low. As indicated in Fig. 9, scenarios 1.1 and 2.1 are those characterized by
449 the lowest CO_2 mass leakages. In scenarios 4.1 (Fig. 9d) and 5.1 (Fig. 9e), considerable amounts
450 of CO_2 leakage are observed when the inclusion permeability is greater than 3.16×10^{-13} m^2
451 ($\log k_2$= -12.5). Broadly, results of these scenarios show that $\%M_{leak}$ is more sensitive to k_{l_1}
452 than k_2, except when permeability of inclusions presents a very high value of k_2 ($\log k_2 \geq$-12.5).
453 These results are aligned with those in González-Nicolás et al. (2015a), which have shown that
454 the permeability of the storage formation has the greatest impact on CO_2 leakage uncertainty,
455 whereas the permeability of passive wells, which can be seen as analogues for inclusions, has a
456 significant influence on CO_2 leakage through the interaction with other parameters (higher order
457 effects), such as the location of the leaky pathways.

458 [Figure 9 here]

459 The $\%M_{leak}$ maps given Fig. 9 can be used in relation to the metric reported by Pacala
460 (2003), which limits the amount of CO_2 leakage returning to the atmosphere to 1% per one year.
461 In scenario 1.1 (Fig. 9a), where the probability of finding an inclusion is the lowest, $\%M_{leak}$
462 would be less than or equal to 1% per one year for values of k_{l_1} greater than 5.01×10^{-14} m^2
463 ($\log k_{l_1} \geq$ -13.3). On the other hand, if P_2 is increased to 0.01 (Fig. 9d), in order to maintain the
464 maximum probable CO_2 leakage below the 1% per year threshold, the minimum permeability
465 required for the injection formation and the inclusions should be 3.98×10^{-13} m^2 ($\log k_{l_1}$= -12.4)
466 and 6.31×10^{-14} m^2 ($\log k_2$= -13.2), respectively.
467 This analysis shows that geostatistical data, such as the probability P_2 and the correlation
468 length, l_{xy}, play a critical role for the probabilistic assessment of CO_2 leakage prior to the GCS
469 development for a candidate reservoir. For instance, Fig. 9 indicates that a probability P_2 greater
470 than 0.001 with l_{xy}= 200 m (scenarios 2.1, 3.1, 4.1, and 5.1) is likely to produce a CO_2 leakage
471 greater than 1% per year, in which case the injections of CO_2 into the candidate storage formation
472 should not be recommended. If the permeability of the storage formation is k_{l_1}= 2.8×10^{-14} m^2
473 ($\log k_{l_1}$= -13.55) (Table 1), injection of CO_2 into the formation is not viable since this would lead
474 to a probability of CO_2 leakage exceeding 1% independently of the P_2 value considered in the
475 scenarios shown in Fig. 9. It is, however, important to emphasize that these estimates are quite
476 conservative since the limit proposed by Pacala (2003) is on CO_2 leakage rates back to the
477 atmosphere, whereas in this study the CO_2 mass leakage considered is the CO_2 that escapes the
478 target storage formation l=1. Additional processes of trapping and attenuation that CO_2 may
479 undergo in the overburden formations are not accounted for.

480 4.3 Combining the Effects of Caprock Inclusions and Passive Wells

481 Uncertainty from permeability of passive wells affects CO_2 mass leakage results when
482 this uncertainty is added to caprock continuity uncertainty, especially in scenarios where CO_2
483 leakage from the caprock discontinuities is expected to be low. Figure 10 and Fig. 11 show CDFs
484 of $\%M_{leak}$ (Eq. (4)) for some of the scenarios described in Table 2 in the cases where uncertainty

485 in passive well is (solid lines) and is not (dashed lines) accounted for. In Fig. 10, the selected
486 inclusion scenarios are those characterized by the same correlation length l_{xy}= 200 m (scenarios
487 2.1, 3.1, 4.1, and 5.1). Results in Fig. 10 reveal that, for the considered test site, uncertainty from
488 permeability of passive wells does not affect significantly CO_2 mass leakage, independently of
489 the prescribed P_2 value, if $\%M_{leak}$ exceeds 1%; yet significant differences are observed for
490 smaller values of $\%M_{leak}$, especially for the lowest probabilities P_2 of the inclusions (e.g., P_2=
491 0.0005 and P_2= 0.001).

492 [Figure 10 here]

493 In Fig. 10, scenario 1.1 (blue lines), which has the lowest inclusion probability P_2, shows
494 an 82% probability of $\%M_{leak}$ to be less than 1×10^{-3} when only caprock continuity uncertainty is
495 considered (blue dashed line). When adding the uncertainty from passive well permeability (blue
496 solid line) this probability is reduced to zero, and there is practical certainty to exceed the 1×10^{-3}
497 threshold. Scenarios 2.1, 3.1, and 4.1 exhibit the same tendency as in scenario 1.1. However,
498 scenarios with higher probability P_2, such as scenario 4.1 (green profile) and 5.1 (in gray), show
499 small differences between their CDFs even for low values of $\%M_{leak}$. Moreover, in scenario 5.1
500 (gray profile) the influence on leakage produced by the uncertainty on the permeability of passive
501 wells is negligible in comparison to the leakage produced through the weak areas of the caprock.
502 Similar to Fig. 10, Fig. 11 shows CDFs of $\%M_{leak}$ (Eq. (4)) for scenarios 2.1, 2.2, 2.3
503 and 2.4 in Table 2, characterized by the same probability P_2 and different correlation lengths,
504 when uncertainty in passive wells is (solid lines) and is not (dashed lines) considered. Results of
505 Fig. 11 indicate that uncertainty on passive wells permeability has an important impact on the
506 CDFs for values of $\%M_{leak}$ below 0.25%, independently of the correlation length. Figure 11 also
507 shows that when uncertainty on passive wells is considered, the influence of the inclusion
508 correlation scale l_{xy}, which practically dictates the size of the inclusions, is noticeable for
509 $\%M_{leak}$ equal to 0.1% and becomes more prominent for $\%M_{leak}$ larger than 1%. On the other

hand, when uncertainty on passive wells is not considered, the influence of l_{xy} is noticed at much lower leakage values ($\%M_{leak}$ = 1×10^{-3}%).

[Figure 11 here]

5 Summary and Conclusions

This work advances a novel methodology for the preliminary assessment of the suitability of saline aquifers for GCS in relation to the risk of CO_2 leakage across high permeable areas of the caprock. The study is focused on inclusion facies but it also considers the presence of passive/abandoned wells of uncertain integrity. This framework is applied to a saline aquifer embedded within the Michigan sedimentary basin, with very limited information on the sealing properties of the caprock. An uncertainty quantification analysis of CO_2 leakage is conducted by developing a Monte Carlo simulation approach, where the caprock permeability field is the major source of uncertainty. Because of the computational cost involved in the use of numerical multiphase flow numerical models, the viability of substituting them with a semi-analytical flow model originally developed to treat leakage from passive wells is studied. To generate caprock discontinuities a two-point geostatistics simulator of permeability is coupled with a clustering algorithm that produces equivalent circular discontinuities for direct use in the semi-analytical flow model. To understand the limitations of applying the semi-analytical model to simulate leakage through large areas of the caprock, a comparison of the semi-analytical algorithm with a numerical code is carried out. Results show that, in general, there is a good agreement between the two models, with the cumulative CO_2 mass leakage produced being practically the same at later times.

Parameters such as D and r_{lc} can be regarded as useful indicators for assessing the vulnerability of any site to CO_2 leakage. Since CO_2 leakage varies greatly depending on P_2 and l_{xy} values, it is critical to prescribe realistic values of P_2 and l_{xy} to be able to quantify uncertainty in CO_2. Uncertainty from passive well permeability has less impact on CO_2 leakage when large

amounts of CO_2 leakage through the inclusions are expected ($\%M_{leak}$ >1%) and is only significant when CO_2 leakages from caprock inclusions are low.

Overall, seemingly low inclusion probabilities P_2, of the order of 1%, may lead to considerable CO_2 leakage. Therefore, extreme caution should be used before injection of CO_2 into the selected candidate formation. While processes of trapping and attenuation that CO_2 may undergo in the overburden formations are expected, to enhance GCS safety, only the collection of high resolution geophysical data over a large area around the injection site may help narrow down the uncertainty on the caprock continuity.

Finally, the methodology presented here can be transferred to assess the probability and intensity of CO_2 leakage in other potential GCS candidate sites in which data on the caprock sealing properties are limited or inexistent. Since this situation is often encountered in the real world, this framework can offer a valid tool to support decision makers in the preliminary selection of safe GCS sites.

6 Acknowledgements

This research was supported by the U. S. Department of Energy, National Energy Technology Laboratory (DOE Project: DE-FE0001830). The research conducted was also made possible with the support of Schlumberger Ltd., who kindly donated the reservoir simulation software suites PETREL and ECLIPSE. The research team is also grateful to Michigan Technological University's Professor Roger Turpening for providing access to the data library regarding the Niagara formations to which this research has been applied, as well as continued support to the use of this library.

7 References

Bachu S (2003) Screening and ranking of sedimentary basins for sequestration of CO_2 in geological media in response to climate change. Environ Geol 44(3):277-289. doi:10.1007/s00254-003-0762-9

560 Baù D, Cody B, González-Nicolás A (2015) An iterative global pressure solution for the semi-
561 analytical simulation of geological carbon sequestration. Computat Geosci 19(4):781-
562 789. doi:10.1007/s10596-015-9489-4
563 Bergman PD, Winter EM (1995) Disposal of carbon-dioxide in aquifers in the US. Energ Convers
564 Manage 36(6-9):523-526. doi:10.1016/0196-8904(95)00058-l
565 Celia MA, Nordbotten JM (2009) Practical modeling approaches for geological storage of carbon
566 dioxide. Ground Water 47(5):627-638. doi:10.1111/j.1745-6584.2009.00590.x
567 Celia MA, Nordbotten JM, Court B, Dobossy M, Bachu S (2011) Field-scale application of a
568 semi-analytical model for estimation of CO_2 and brine leakage along old wells. Int J
569 Greenh Gas Con 5(2):257-269. doi:10.1016/j.ijggc.2010.10.005
570 Celia MA, Bachu S, Nordbotten JM, Bandilla K (2015) Status of CO_2 storage in deep saline
571 aquifers with emphasis on modeling approaches and practical simulations. Water Resour
572 Res 51(9):6846-6892. doi:10.1002/2015WR017609
573 Chang KW, Minkoff S, Bryant S (2008) Modeling leakage through faults of CO_2 stored in an
574 aquifer. SPE Annual Technical Conference and Exhibition. Society of Petroleum
575 Engineers. doi:10.2118/115929-ms
576 Deutsch CV, Journel AG (1998) GSLIB: geostatistical software library and user's guide. New
577 York : Oxford University Press, Version 2.0, 2nd ed.
578 Gasda SE, Bachu S, Celia MA (2004) Spatial characterization of the location of potentially leaky
579 wells penetrating a deep saline aquifer in a mature sedimentary basin. Environ Geol 46(6-
580 7):707-720. doi:10.1007/s00254-004-1073-5
581 González-Nicolás A, Baù D, Cody BM, Alzraiee A (2015a) Stochastic and global sensitivity
582 analyses of uncertain parameters affecting the safety of geological carbon storage in
583 saline aquifers of the Michigan Basin. Int J Greenh Gas Con 37:99-114.
584 doi:10.1016/j.ijggc.2015.03.008
585 González-Nicolás A, Baù D, Alzraiee A (2015b) Detection of potential leakage pathways from
586 geological carbon storage by fluid pressure data assimilation. Adv Water Resour 86:366-
587 384. doi:10.1016/j.advwatres.2015.10.006

588 Goovaerts P (1997) Geostatistics for natural resources evaluation. Applied Geostatistics Series,
589 Oxford University Press on Demand, New York
590 Grana D, Mukerji T, Dovera L, Della Rossa E (2012) Sequential simulations of mixed discrete-
591 continuous properties: Sequential Gaussian mixture simulation, Geostatistics Oslo 2012.
592 Springer, pp. 239-250
593 Hahn GJ (1967) Statistical models in engineering. Wiley series on systems engineering and
594 analysis. Wiley, New York
595 Halliburton (1990) Log 21101375660000 Stech Upper Half (Date: 09/04/1990)
596 International Energy Agency (2008) Carbon capture and storage: meeting the challenge of climate
597 change. IEA/OECD. Paris
598 Journel AG, Alabert F (1989) Non-Gaussian data expansion in the Earth sciences. Terra Nova 1
599 (2):123-134. doi:10.1111/j.1365-3121.1989.tb00344.x
600 Kopp A, Binning PJ, Johannsen K, Helmig R, Class H (2010) A contribution to risk analysis for
601 leakage through abandoned wells in geological CO_2 storage. Adv Water Resour
602 33(8):867-879. doi:10.1016/j.advwatres.2010.05.001
603 Krige DG (1951) A statistical approach to some mine valuations and allied problems on the
604 Witwatersrand. M.Sc. Eng. Thesis of University of Witwatersrand, Johannesburg
605 MDEQOGD (2014) Michigan Department of Environmental Quality Oil and Gas Database,
606 http://www.michigan.gov/deq/0,4561,7-135-6132_6828-98518--,00.html. Accessed
607 03/08/2014. http://www.michigan.gov/deq/0,4561,7-135-6132_6828-98518--,00.html
608 Metz B, Intergovernmental Panel on Climate Change. Working Group III. (2005) IPCC Special
609 report on carbon dioxide capture and storage. Cambridge University Press, for the
610 Intergovernmental Panel on Climate Change, Cambridge
611 Nicholls N, Gruza G, Jouzel J, Karl T, Ogallo L, Parker D (1996) Observed climate variability
612 and change. Cambridge University Press
613 Nogues JP, Court B, Dobossy M, Nordbotten JM, Celia MA (2012) A methodology to estimate
614 maximum probable leakage along old wells in a geological sequestration operation. Int J
615 Greenh Gas Con 7:39-47. doi:10.1016/j.ijggc.2011.12.003

616 Nordbotten JM, Celia MA, Bachu S, Dahle HK (2005) Semianalytical solution for CO_2 leakage
617 through an abandoned well. Environ Sci Technol 39(2):602-611. doi: 10.1021/es035338i
618 Nordbotten JM, Kavetski D, Celia MA, Bachu S (2009) Model for CO_2 leakage including multiple
619 geological layers and multiple leaky wells. Environ Sci Technol 43(3):743-749. doi:Doi
620 10.1021/Es801135v
621 Pacala SW (2003) Global constraints on reservoir leakage. In: Gale J, Kaya Y (eds) Greenhouse
622 Gas Control Technologies – 6th International Conference. Pergamon, Oxford, pp 267-
623 272. doi:http://dx.doi.org/10.1016/B978-008044276-1/50043-X
624 Ruether JA (1998) FETC Programs for reducing greenhouse gas emissions. (No. DOE/FETC-
625 98/1058). USDOE Federal Energy Technology Center, Pittsburgh, PA (United States)
626 Sakamoto Y, Tanaka A, Tenma N, Komai T (2011) Numerical study on flow behavior of CO_2 in
627 an aquifer for risk assessment of carbon capture and storage. Energy Procedia 4:4170-
628 4177. doi:10.1016/j.egypro.2011.02.363
629 SCH (1983) Log 21101365880000 Burch Main Suite (Date 06/19/1983)
630 SCH (1991) Log 21101375660000 Stech Lower Half (Date: 06/29/1991)
631 Schlumberger (2010) Eclipse technical description, v. 2010.1, Report, Abingdon, U.K.
632 Solomon S, Intergovernmental Panel on Climate Change., Intergovernmental Panel on Climate
633 Change. Working Group I. (2007) Climate change 2007: the physical science basis:
634 contribution of Working Group I to the Fourth Assessment Report of the
635 Intergovernmental Panel on Climate Change. Cambridge University Press, Cambridge;
636 New York
637 Trebin FA (1945) Permeability to oil of sandstone reservoir. Gostoptekhizdat, Moscow
638 Turpening R, Toksöz M, Born A, al. e (1992) Reservoir delineation consortium annual report,
639 Massachusetts Institute of Technology, Cambridge
640 Van Genuchten MT (1980) A closed-form equation for predicting the hydraulic conductivity of
641 unsaturated soils. Soil Sci Soc Am J 44(5):892-898.
642 doi:10.2136/sssaj1980.03615995004400050002x

643 Zhang Y, Oldenburg CM, Finsterle S (2010) Percolation-theory and fuzzy rule-based probability
644 estimation of fault leakage at geologic carbon sequestration sites. Environ Earth Sci
645 59(7):1447-1459. doi:10.1007/s12665-009-0131-4
646 Zhou Q, Birkholzer JT, Mehnert E, Lin Y-F, Zhang K (2009) Modeling basin- and plume-scale
647 processes of CO_2 storage for full-scale deployment. Ground Water 48(4):494-514.
648 doi:10.1111/j.1745-6584.2009.00657.x

649 **List of captions from Tables and Figures**

650

651 **Table 1** Hydro-geomechanical parameters
652
653
654 **Table 2** Parameters used for the generation of caprock fields. All considered scenarios are
655 assumed to have a correlation length l_{k_1}=1,000 m for facies 1

656

657 **Fig. 1** Representation of the clustering approach. In this example, the number of 84 inclusions-
658 blocks (in orange) is reduced to 16 clusters (black circles). Limit of the hydrocarbon reservoir
659 (red gridblocks) is shown by the blue line (Brown Niagaran pinnacle in Fig. 3)

660

661 **Fig 2**. Flow chart of the methodology

662

663 **Fig. 3** Cross-section of the Michigan Basin test site proposed for GCS (Turpening et al., 1992).
664 The candidate formation is highlighted in yellow and the caprock is colored in green

665

666 **Fig. 4** Locations of 60 passive wells that cross the candidate GCS formation of the Michigan
667 Basin (black crosses) and of the 20 equivalent clusters (blue circles). The red dot indicates the
668 position of the proposed injection well (Merit 1-20A in Fig. 3)

669

Fig. 5 Panels **a** and **b**: caprock permeability for two representative realizations of scenario 3.1. Panels **c** and **d**: ECLIPSE and ELSA-IGPS comparison of CO_2 mass leakage over time for realizations in **a** and **b**, respectively

Fig. 6 CDFs of $\%M_{leak}$ for ELSA-IGPS (in red) and ECLIPSE (blue) of scenario 2.1 and scenario 4.1

Fig. 7 a Relationship between correlation length and the average distance between cluster centers and injection well and **b** relationship between correlation length and the inclusion ratio

Fig. 8 CDF of $\%M_{leak}$ for several scenarios described in Table 2

Fig. 9 Maps of the 95th percentile of $\%M_{leak}$ as a function of the injection formation permeability (k_{l_1}) and the inclusions permeability (k_2) for **a** scenario 1.1, **b** scenario 2.1, **c** scenario 3.1, **d** scenario 4.1, and **e** scenario 5.1

Fig. 10 CDF of $\%M_{leak}$ for some scenarios characterized by different probability P_2 and the same correlation length in the cases where uncertainty in passive well is (solid lines) and is not (dashed lines) accounted for

Fig. 11 CDFs of $\%M_{leak}$ for scenarios 2.1 to 2.4 in Table 2, characterized by the same probability P_2 and different correlation lengths when uncertainty in passive well is (solid lines) and is not (dashed lines) considered

694

695 **Table 1** Hydro-geomechanical parameters

Parameter	Symbol	Value	Units
Brine density	ρ_b	1,045	kg m^{-3}
CO_2 density	ρ_c	575	kg m^{-3}
Brine viscosity	μ_b	4.5×10^{-4}	Pa s
CO_2 viscosity	μ_c	4.6×10^{-5}	Pa s
System compressibility	c_{eff}	4.6×10^{-10}	Pa^{-1}
Injected aquifer porosity	φ_{l_1}	0.084	/
Overlying aquifer porosity	φ_{l_2}	0.05	/
Brine residual saturation	s_b^{res}	0.3	/
End-point CO_2 relative permeability	$k_{r,c0}$	0.42	/
Injection aquifer permeability	k_{l_1}	2.8×10^{-14}	m^2
Overlying aquifer permeability	k_{l_2}	9.6×10^{-15}	m^2
Sealing formation permeability	k_1	0	m^2
Weak areas/inclusions permeability	k_2	2.8×10^{-14}	m^2

696

Table 2 Parameters used for the generation of caprock fields. All considered scenarios are assumed to have a correlation length l_{k_1}=1,000 m for facies 1

Scenario	Covariance model	N_{MC}	P_2*	l_{xy} (m)
1.1	Exponential	500	0.0005	200
1.2				400
1.3				600
1.4				1,500
2.1	Exponential	500	0.001	200
2.2				400
2.3				600
2.4				1,500
3.1	Exponential	500	0.005	200
3.2				400
3.3				600
3.4				1,500
4.1	Exponential	500	0.01	200
4.2				400
4.3				600
4.4				1,500
5.1	Exponential	500	0.02	200
5.2				400
5.3				600
5.4				1,500

*Facies 2 corresponds to inclusions. Probability of facies 1 (perfectly sealing formation) is $P_1 = 1 - P_2$.

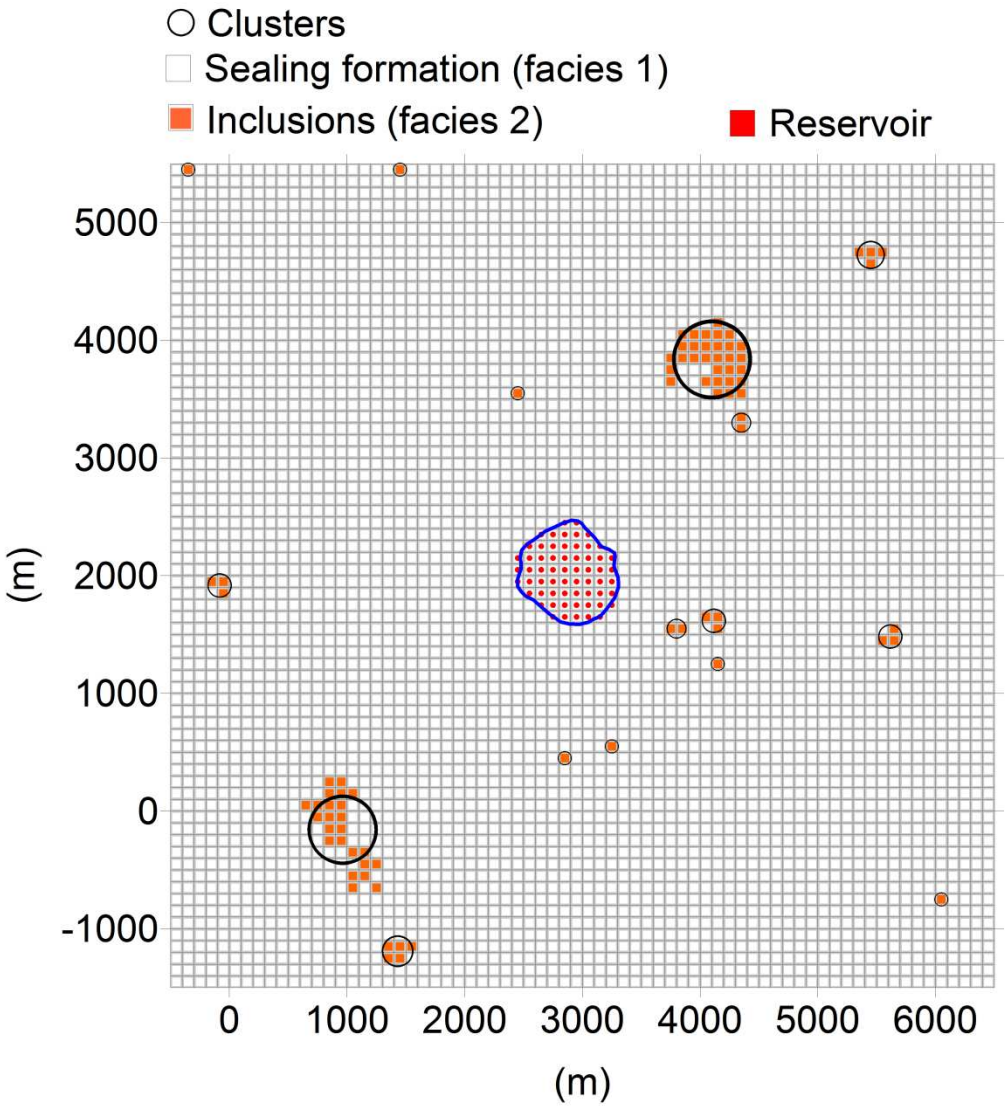

Fig. 1 Representation of the clustering approach. In this example, the number of 84 inclusions-blocks (in orange) is reduced to 16 clusters (black circles). Limit of the hydrocarbon reservoir (red gridblocks) is shown by the blue line (Brown Niagaran pinnacle in Fig. 3)

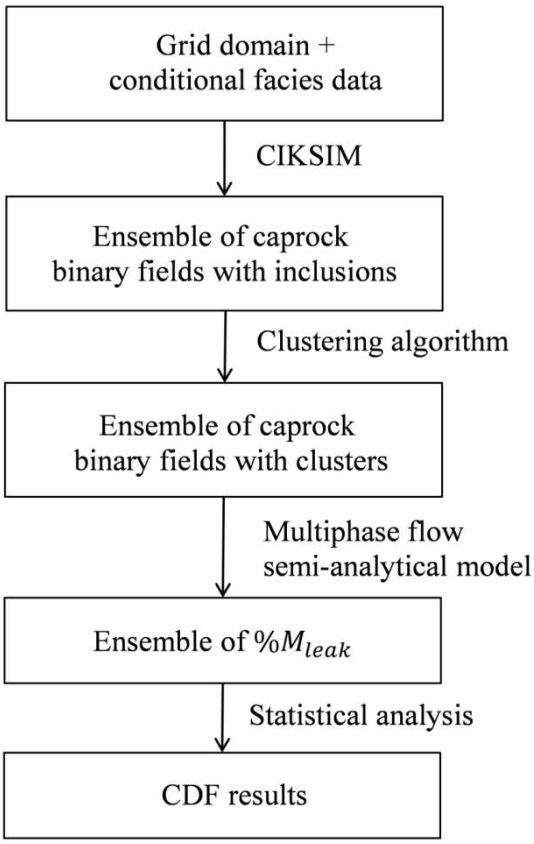

707
708 **Fig 2**. Flow chart of the methodology

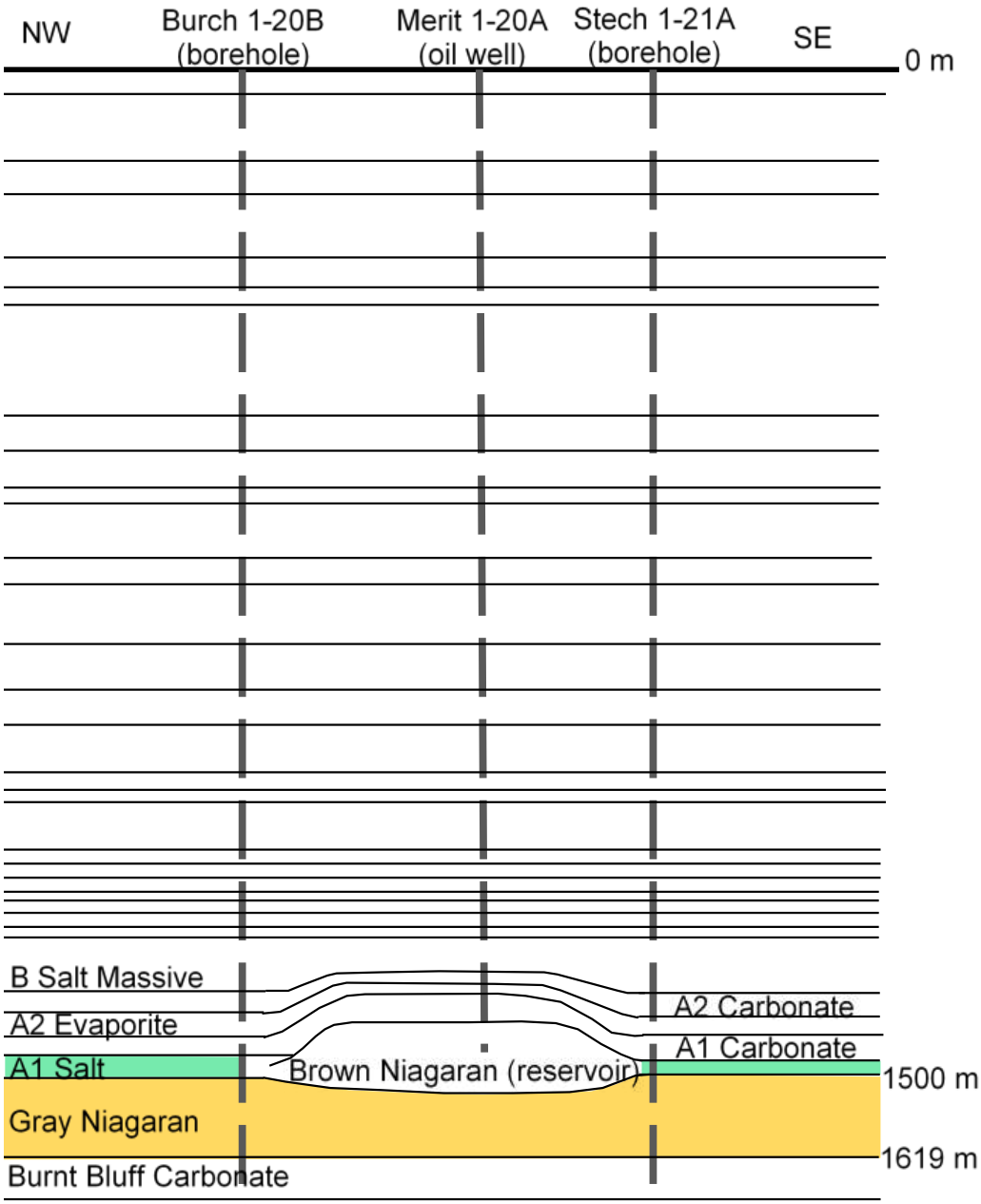

709

710 **Fig. 3** Cross-section of the Michigan Basin test site proposed for GCS (Turpening et al., 1992).

711 The candidate formation is highlighted in yellow and the caprock is colored in green

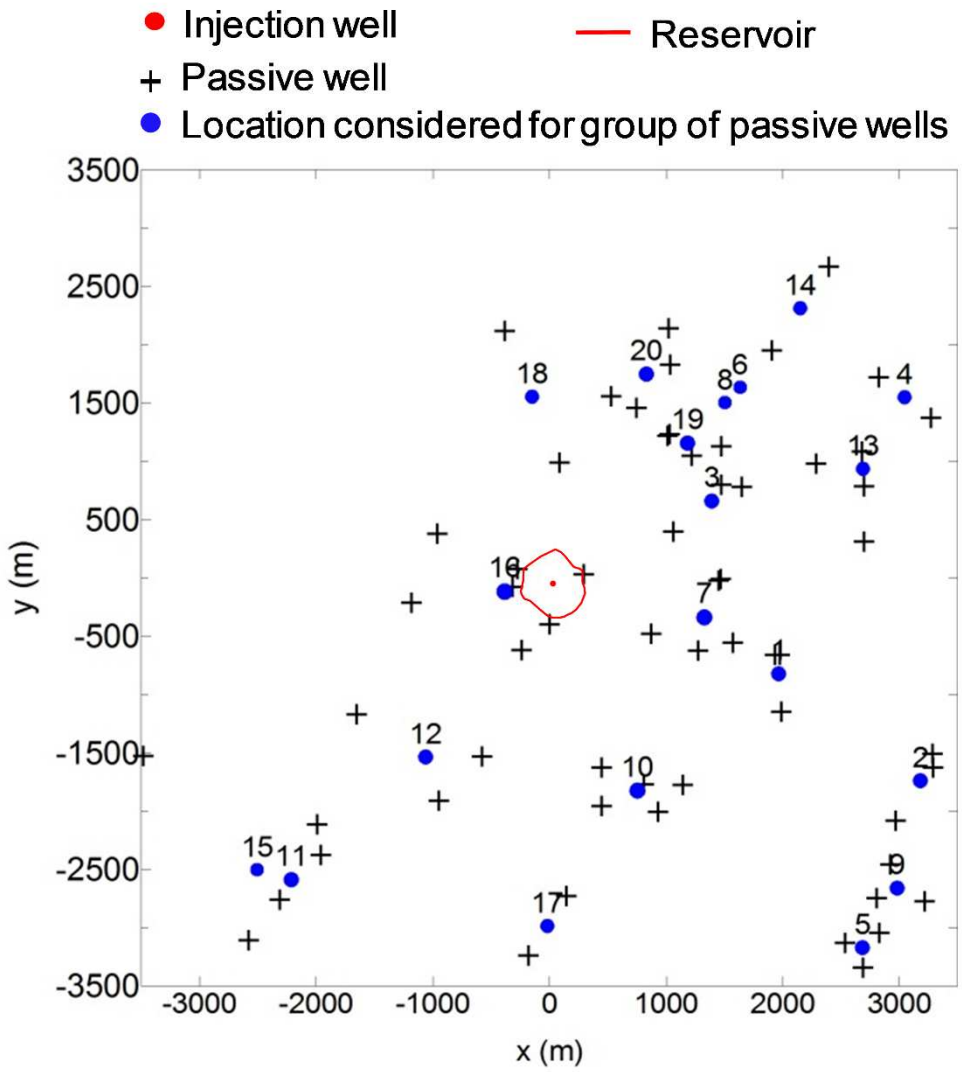

712

713 **Fig. 4** Locations of 60 passive wells that cross the candidate GCS formation of the Michigan
714 Basin (black crosses) and of the 20 equivalent clusters (blue circles). The red dot indicates the
715 position of the proposed injection well (Merit 1-20A in Fig. 3)

716

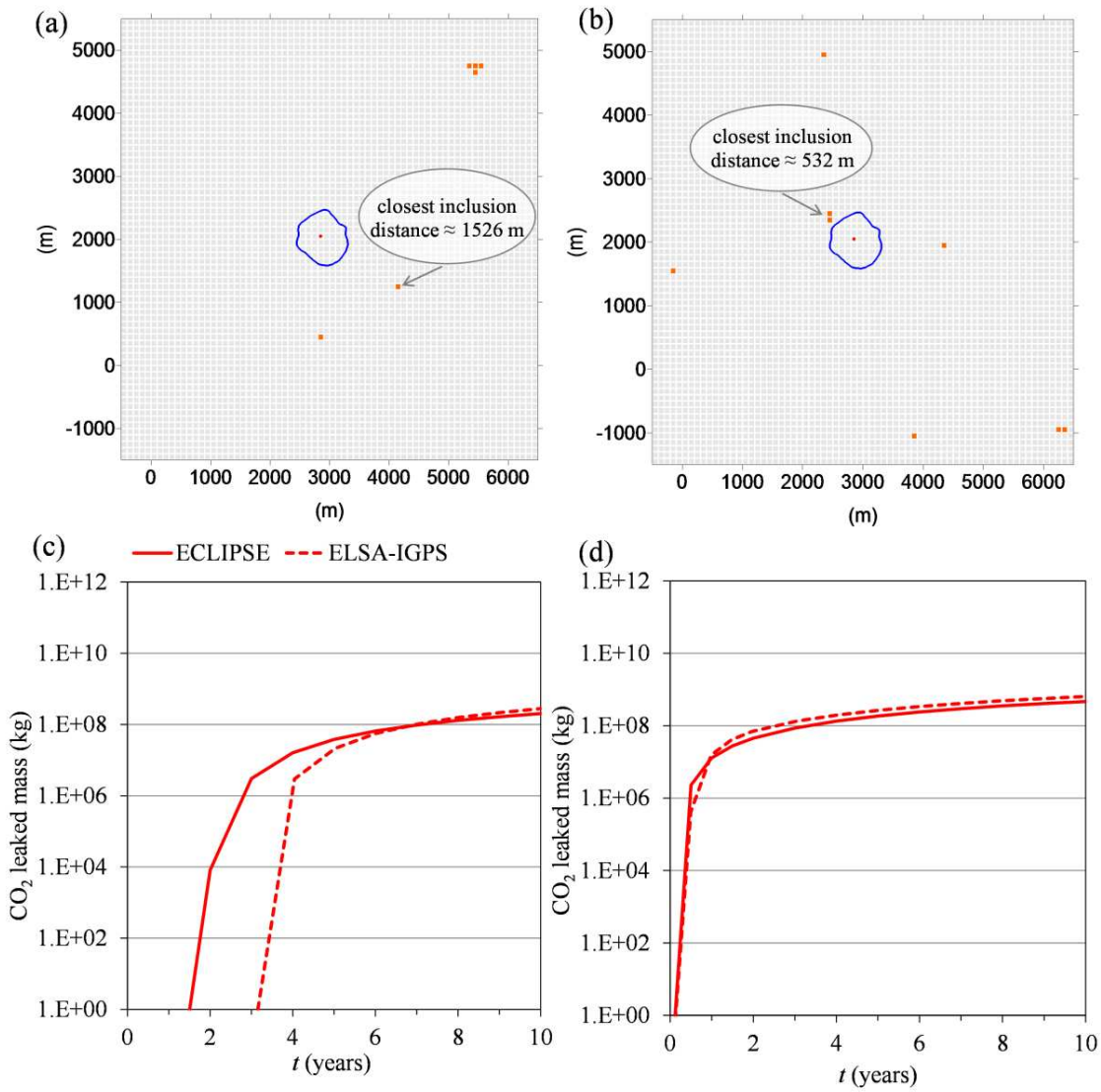

717

718 **Fig. 5** Panels **a** and **b**: caprock permeability for two representative realizations of scenario 3.1.

719 Panels **c** and **d**: ECLIPSE and ELSA-IGPS comparison of CO_2 mass leakage over time for

720 realizations in **a** and **b**, respectively

721

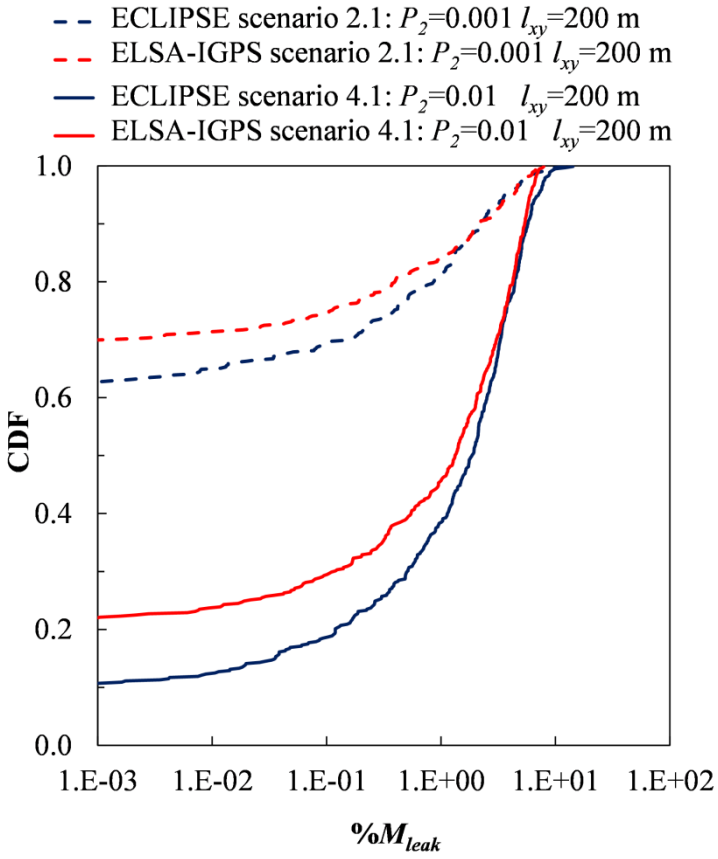

722
723 **Fig. 6** CDFs of %M_{leak} for ELSA-IGPS (in red) and ECLIPSE (blue) of scenario 2.1 and scenario
724 4.1
725

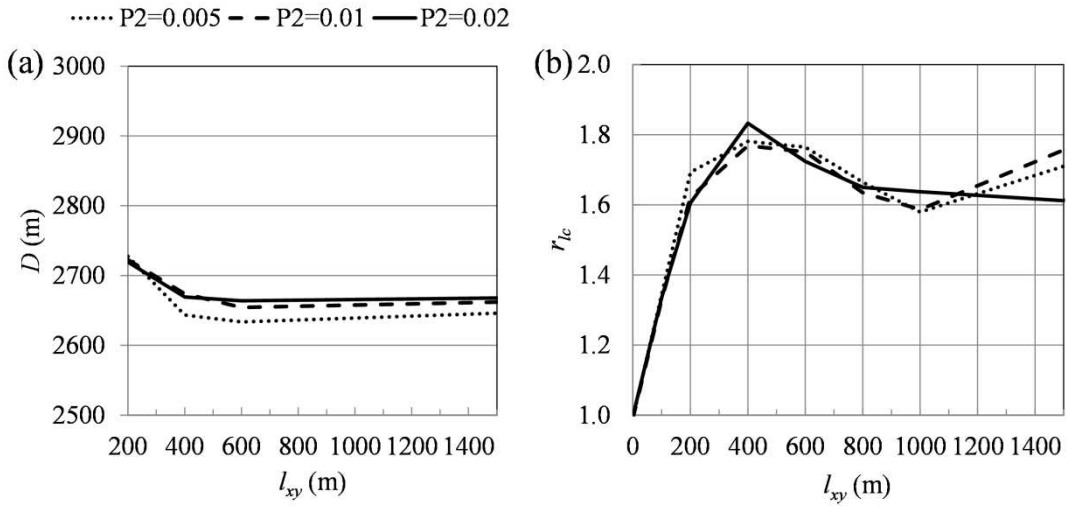

726

727 **Fig. 7 a** Relationship between correlation length and the average distance between cluster centers

728 and injection well and **b** relationship between correlation length and the inclusion ratio

729

730

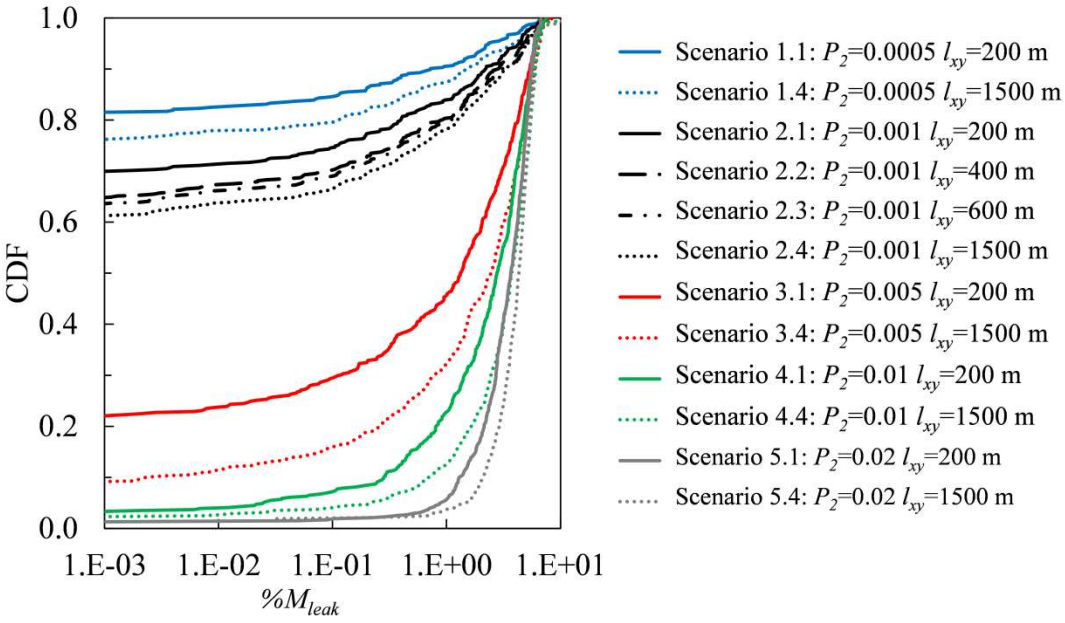

731

732 **Fig. 8** CDF of $\%M_{leak}$ for several scenarios described in Table 2

733

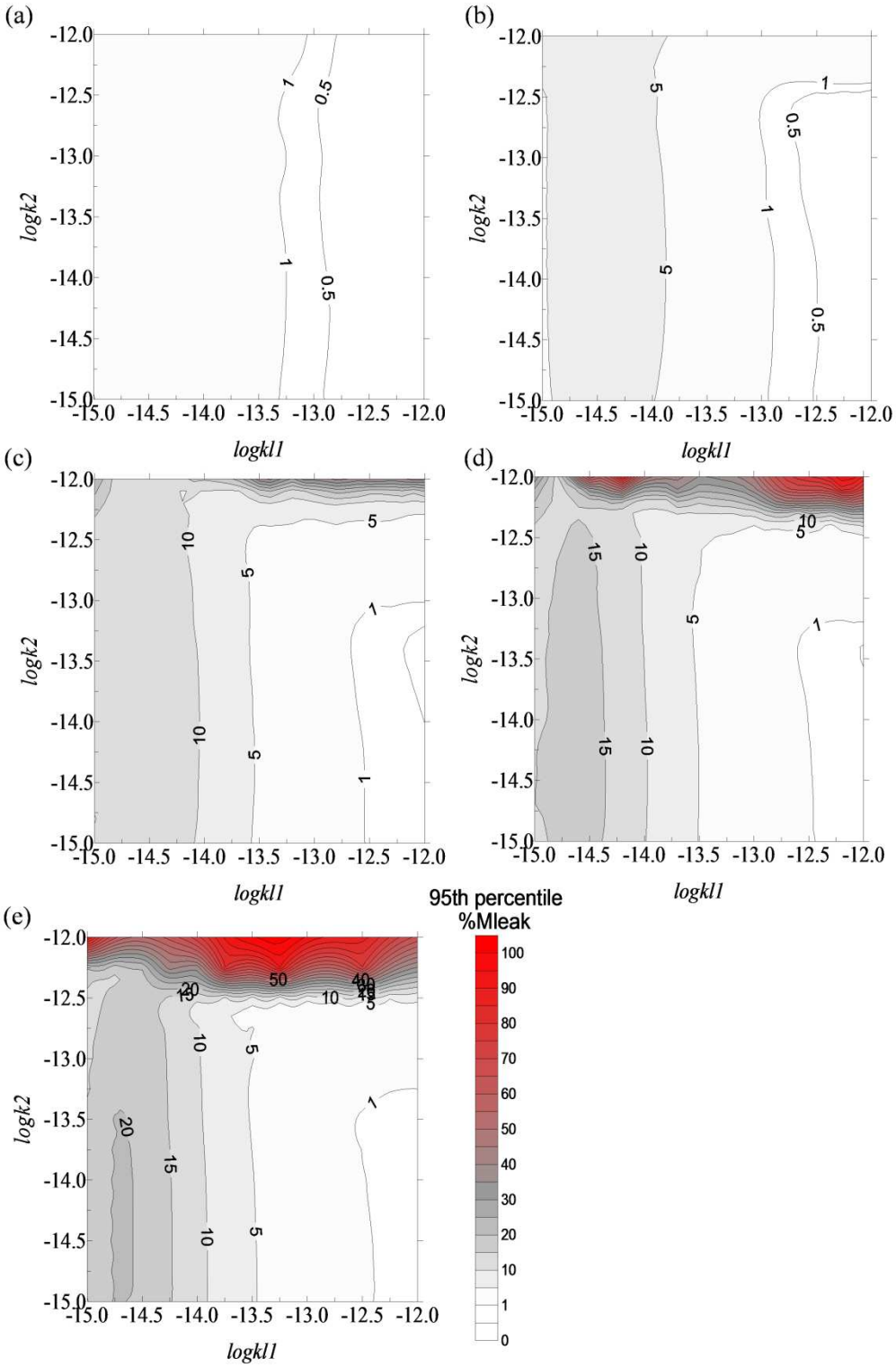

734

735 **Fig. 9** Maps of the 95th percentile of $\%M_{leak}$ as a function of the injection formation permeability

736 (k_{l_1}) and the inclusions permeability (k_2) for **a** scenario 1.1, **b** scenario 2.1, **c** scenario 3.1, **d**

737 scenario 4.1, and **e** scenario 5.1

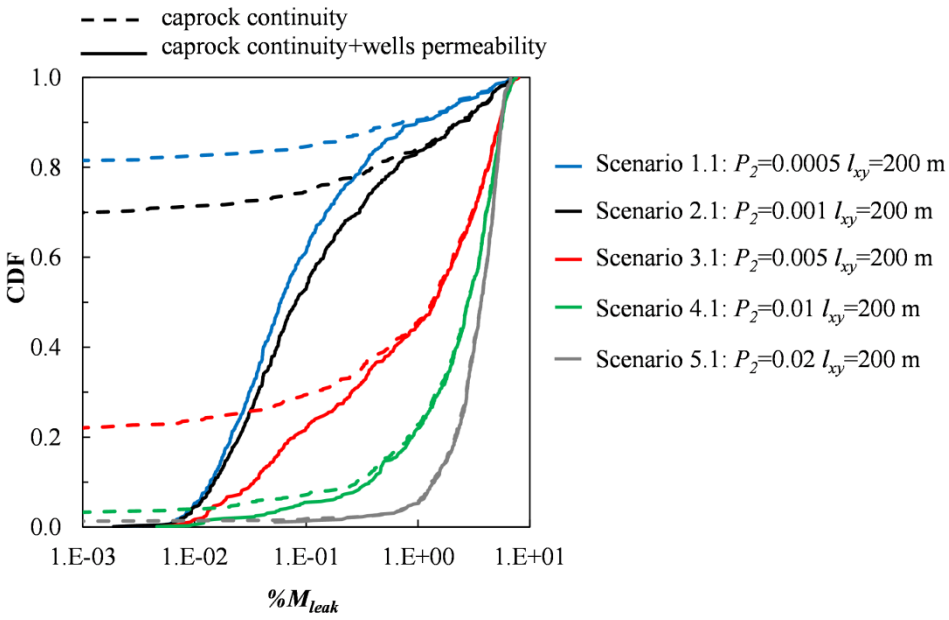

Fig. 10 CDF of $\%M_{leak}$ for some scenarios characterized by different probability P_2 and the same correlation length in the cases where uncertainty in passive well is (solid lines) and is not (dashed lines) accounted for

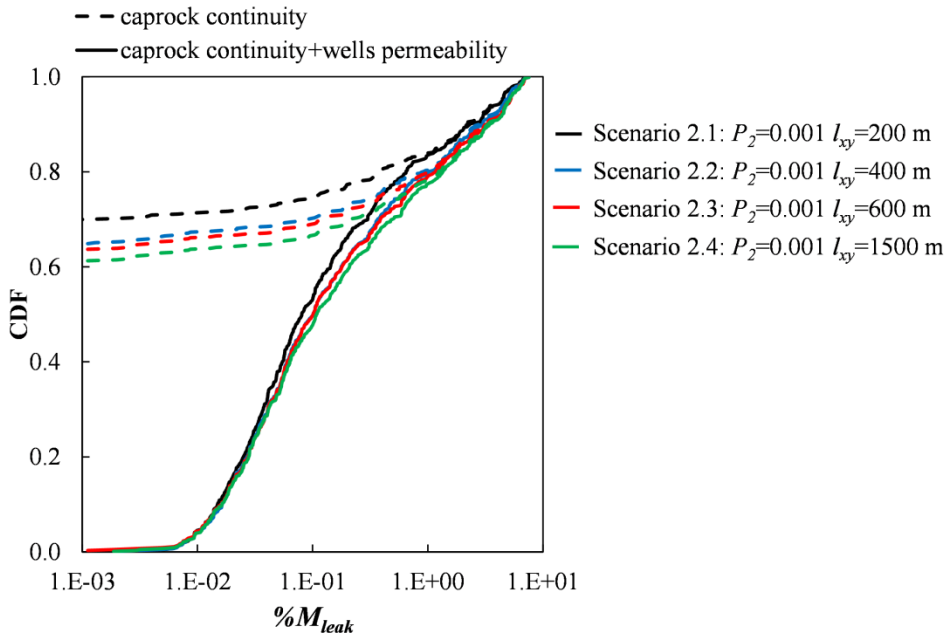

Fig. 11 CDFs of $\%M_{leak}$ for scenarios 2.1 to 2.4 in Table 2, characterized by the same probability P_2 and different correlation lengths when uncertainty in passive well is (solid lines) and is not (dashed lines) considered